Journal of Computational Physics 345 (2017) 245–259

Contents lists available at ScienceDirect

Journal of Computational Physics

www.elsevier.com/locate/jcp

Improvement and performance evaluation of the perturbation source method for an exact Monte Carlo perturbation calculation in fixed source problems

Hiroki Sakamoto [a], Toshihiro Yamamoto [b,*]

[a] Transnuclear Tokyo, Ltd., 1-18-16, Shinbashi, Minato-ku, Tokyo, 105-0004, Japan
[b] Research Reactor Institute, Kyoto University, 2 Asashiro Nishi, Kumatori-cho, Sennan-gun, Osaka, 590-0494, Japan

ARTICLE INFO

Article history:
Received 26 September 2016
Received in revised form 24 January 2017
Accepted 5 May 2017
Available online 17 May 2017

Keywords:
Monte Carlo
Perturbation
Fixed source problem
Transport equation

ABSTRACT

This paper presents improvement and performance evaluation of the "perturbation source method", which is one of the Monte Carlo perturbation techniques. The formerly proposed perturbation source method was first-order accurate, although it is known that the method can be easily extended to an exact perturbation method. A transport equation for calculating an exact flux difference caused by a perturbation is solved. A perturbation particle representing a flux difference is explicitly transported in the perturbed system, instead of in the unperturbed system. The source term of the transport equation is defined by the unperturbed flux and the cross section (or optical parameter) changes. The unperturbed flux is provided by an "on-the-fly" technique during the course of the ordinary fixed source calculation for the unperturbed system. A set of perturbation particle is started at the collision point in the perturbed region and tracked until death. For a perturbation in a smaller portion of the whole domain, the efficiency of the perturbation source method can be improved by using a virtual scattering coefficient or cross section in the perturbed region, forcing collisions. Performance is evaluated by comparing the proposed method to other Monte Carlo perturbation methods. Numerical tests performed for a particle transport in a two-dimensional geometry reveal that the perturbation source method is less effective than the correlated sampling method for a perturbation in a larger portion of the whole domain. However, for a perturbation in a smaller portion, the perturbation source method outperforms the correlated sampling method. The efficiency depends strongly on the adjustment of the new virtual scattering coefficient or cross section.

1. Introduction

Monte Carlo methods have difficulties in calculating the effect of a small perturbation in the system parameters. The effect of a perturbation, of course, can be obtained by performing two independent Monte Carlo calculations and subtracting the estimates of the unperturbed system from those of the perturbed system. A prohibitively huge computational cost would however be required to obtain statistically significant estimates for a small perturbation. The statistical uncertainty of the difference between two independent runs is sometimes comparable with the change of the estimates if the perturbation is small and the computation time short. Thus far, two perturbation calculation methods, the correlated sampling method

* Corresponding author. Fax: +81 72 451 2658.
E-mail address: toshihiro.yamamoto223@gmail.com (T. Yamamoto).

http://dx.doi.org/10.1016/j.jcp.2017.05.004
0021-9991/

[1–5] and the differential operator sampling method [4,6,7], have been developed to overcome difficulties in the Monte Carlo perturbation calculations. These methods have been widely investigated; their unique advantages and drawbacks have been identified in many publications (e.g., [8–12]).

In the correlated sampling method, the perturbed history is forced to follow the unperturbed one along the same tracks in phase space. It has been found that the correlated sampling method suffers from a large or unbounded variance when the perturbation exceeds a certain limit [4].

The differential operator sampling method accumulates a sum of products combining cross section, path segment probabilities, and associated partial derivatives (first order and higher) for all trajectories. The divergence of the variance, which frequently occurs in the correlated sampling method for a larger perturbation, can be circumvented in the differential operator method. However, the differential operator sampling method uses up to the second-order terms in a widely used Monte Carlo code, MCNP [12], and the higher-order terms, beyond the third order, are truncated. A localized and large perturbation would require higher-order terms, truncated in commonly-used differential operator sampling method. As the order becomes higher, the mathematical formulation of the higher-order terms becomes more involved. In addition, many quantities need to be scored during the course of the particle's random walk, making the calculation less efficient. In the Monte Carlo code, MVP, the order of the differential operator method is uniquely expanded to the 8th order [9]. However higher the order is, the differential operator sampling method remains essentially approximate and may be occasionally insufficient for large and localized perturbations.

The two Monte Carlo perturbation methods have already been implemented into some Monte Carlo production codes [8,9,12–16]. The two Monte Carlo perturbation methods can be applied to perturbation calculations in k_{eff}-eigenvalue problems as well as fixed source problems. In the k_{eff}-eigenvalue problems, the fission source spatial distribution is also perturbed due to the perturbation of system parameters such as cross sections and material density. To estimate the effect of the fission source perturbation, some techniques have been developed and installed into Monte Carlo codes [8,9,17]. For the fixed source problems, on the other hand, the need to consider the fission source perturbation effect can be avoided.

Besides the correlated sampling method and the differential operator method, there exists another perturbation method known as the "perturbation source" method [18–20] in which a separate random walk is performed to follow a "perturbation particle" once a perturbed region is encountered in the original random walk. The perturbation particle explicitly represents the change of the flux due to the perturbation. However, this method is less effective when a large number of collisions occurs in the perturbed region during a history, too many perturbation particles must be followed. On the other hand, if the perturbed region is very small, most of particles pass through the perturbed region without collision and too few perturbation particles are started, which make the perturbation source method less effective than other perturbation techniques. To compensate for the shortcomings of the perturbation source method, Preeg and Tsang [20] proposed a hybrid method that uses the correlated sampling method initially, and then switches to the perturbation source method for the remainder of the history. According to [18,19], the perturbation source method has been used within the first-order accuracy by neglecting higher-order terms; although it is known that the method can be easily extended to an exact perturbation method [18]. Thus, the formerly proposed perturbation source method only yields an approximate estimate of perturbation.

The present paper focuses on the Monte Carlo perturbation method for particle (light or neutron) transport in a semi-transparent material. The perturbation source method is improved to take into account higher-order terms neglected in the previous studies. This paper proposes a method for improving the effectiveness of the perturbation source method to estimate the variation of flux in problems where the perturbed region covers only a small fraction of the whole domain. The dependence of the efficiency improvement for a user-specified parameter is investigated. It is shown that the newly improved perturbation source method outperforms the correlated sampling method and the differential operator method for such problems in terms of computation efficiency. The underlying concept of this paper is applicable to other particle transport calculations. In the sections that follow, the theory and numerical examples are presented.

2. Theory of the improved perturbation source method

This section presents a theory of the perturbation method used to calculate the difference of flux variation caused by the perturbation of system parameters in a fixed source problem. The theory is already proposed [18,19] and simple, but it provides an exact perturbation method that can be performed in the Monte Carlo method. The unperturbed light transport equation with a fixed source is given by

$$\mathbf{H}\phi(\mathbf{r},\boldsymbol{\Omega},E)=S(\mathbf{r},\boldsymbol{\Omega},E), \tag{1}$$

where

$$\mathbf{H}\phi(\mathbf{r},\boldsymbol{\Omega},E)\equiv\boldsymbol{\Omega}\cdot\nabla\phi(\mathbf{r},\boldsymbol{\Omega},E)+\mu_t(\mathbf{r},E)\phi(\mathbf{r},\boldsymbol{\Omega},E)-\int_{4\pi}d\boldsymbol{\Omega}'\int dE'\mu_s\big(\mathbf{r},\boldsymbol{\Omega}'\to\boldsymbol{\Omega},E'\to E\big)\phi\big(\mathbf{r},\boldsymbol{\Omega}',E'\big), \tag{2}$$

$\phi(\mathbf{r},\boldsymbol{\Omega},E)=$ the unperturbed flux at position $\mathbf{r}$ with energy E and direction $\boldsymbol{\Omega}$, $S(\mathbf{r},\boldsymbol{\Omega},E)=$ the external light source term, $\mu_t=$ the total coefficient of absorption and scattering, $\mu_s=$ the scattering coefficient. We suppose that the coefficients in Eq. (2) are perturbed with the fixed source term being unchanged. Then, the flux is perturbed to $\phi'(\mathbf{r},\boldsymbol{\Omega},E)(\equiv\phi(\mathbf{r},\boldsymbol{\Omega},E)+$

$\delta\phi(\mathbf{r}, \boldsymbol{\Omega}, E))$ where $\delta\phi(\mathbf{r}, \boldsymbol{\Omega}, E)$ is the difference of the flux due to the perturbation. On the other hand, the perturbed flux, $\phi'(\mathbf{r}, \boldsymbol{\Omega}, E)$, obeys the following perturbed transport equation:

$$\mathbf{H}\phi'(\mathbf{r}, \boldsymbol{\Omega}, E) + \Delta\mathbf{H}\phi'(\mathbf{r}, \boldsymbol{\Omega}, E) = S(\mathbf{r}, \boldsymbol{\Omega}, E). \tag{3}$$

$\Delta\mathbf{H}\phi(\mathbf{r}, \boldsymbol{\Omega}, E)$ is described by

$$\Delta\mathbf{H}\phi(\mathbf{r}, \boldsymbol{\Omega}, E) \equiv \Delta\mu_t(\mathbf{r}, E)\phi(\mathbf{r}, \boldsymbol{\Omega}, E) - \int_{4\pi} d\boldsymbol{\Omega}' \int dE' \Delta\mu_s\big(\mathbf{r}, \boldsymbol{\Omega}' \to \boldsymbol{\Omega}, E' \to E\big)\phi\big(\mathbf{r}, \boldsymbol{\Omega}', E'\big), \tag{4}$$

where $\Delta\mu_t$ and $\Delta\mu_s$ are the differences of the total coefficient and the scattering coefficient due to the perturbation, respectively. Subtracting Eq. (1) from Eq. (3) yields the transport equation for the flux difference $\delta\phi(\mathbf{r}, \boldsymbol{\Omega}, E)$:

$$\mathbf{H}\delta\phi(\mathbf{r}, \boldsymbol{\Omega}, E) + \Delta\mathbf{H}\delta\phi(\mathbf{r}, \boldsymbol{\Omega}, E) = -\Delta\mathbf{H}\phi(\mathbf{r}, \boldsymbol{\Omega}, E). \tag{5}$$

The right-hand side of Eq. (5) represents a source term for this equation and is defined by Eq. (4). To solve Eq. (5), the unperturbed flux $\phi(\mathbf{r}, \boldsymbol{\Omega}, E)$ on the right-hand side of Eq. (5) needs to be obtained by the unperturbed transport equation, Eq. (1), with the fixed source $S(\mathbf{r}, \boldsymbol{\Omega}, E)$. Once we know the unperturbed flux and the source term for Eq. (5), the flux difference $\delta\phi(\mathbf{r}, \boldsymbol{\Omega}, E)$ can be obtained by solving Eq. (5).

Formerly, the perturbation source method was used by omitting the second term on the left-hand side of Eq. (5) [18,19]. However, it is very easy to include this term by transporting perturbation particles in the *perturbed* system, not in the unperturbed system as noted in [18]. This perturbation method that solves Eq. (5) can provide an exact flux difference without approximation. When we apply this perturbation method to a deterministic method, the unperturbed flux distribution is calculated first and then it is stored in a memory or a file. Then, Eq. (5) is solved by reading the unperturbed flux distribution from the file or memory. As can be seen in Eq. (4), the flux is energy- and angular-dependent to estimate the source term in Eq. (5). Thus, if a three dimensional problem with a fine energy group structure is being treated, a huge memory or file storage would be required. We have to note that the source term can be positive and negative, thereby making the flux difference positive and negative as well.

3. Monte Carlo algorithm of the perturbation source method

3.1. Monte Carlo algorithm for calculating flux difference

This section presents a Monte Carlo algorithm to solve the flux difference transport equation, Eq. (5). First of all, a fixed source Monte Carlo calculation is performed to solve Eq. (1), and the unperturbed flux $\phi(\mathbf{r}, \boldsymbol{\Omega}, E)$ is obtained. This calculation is called the "fixed source calculation mode". Up to this point, this procedure is similar to ordinary fixed source calculations. When a particle undergoes a collision in the perturbed region, the source term for the flux difference equation, Eq. (5), is estimated. The information for the source term is composed of the position, energy, direction, and particle weight. Two methods are available for obtaining the source term. One method is to perform the unperturbed fixed source calculation until a sufficiently large number of collision points are accumulated. After the unperturbed fixed source calculation is completed, the accumulated seven-dimensional data (3 for position, 1 for energy, 2 for direction, and 1 for particle weight) are used for the subsequent flux difference calculation for Eq. (5). This method, however, requires a large storage capacity to store a sufficient amount of source information. This is more serious in the Monte Carlo method since a collision point is defined in the continuous space while the flux is allocated at discrete points in the deterministic methods.

Another method, which is adopted in this paper, is a so-called "on-the-fly" technique. When a particle undergoes a collision in the perturbed region in the *unperturbed* system, the fixed source calculation is temporarily suspended. Then, the source term for Eq. (5) is calculated using Eq. (4) and a new particle (perturbation particle), which represents the flux difference, is emitted from the collision point (how to determine the weight, energy, and direction of the new particle is described below). This process is called the "perturbation calculation mode". The perturbation particle is tracked using the *perturbed* parameters as defined on the left-hand side of Eq. (5). The proposed perturbation method can yield the exact values of the flux change on the grounds that the perturbed parameters are used for tracking the perturbation particle. After the perturbation particle emitted from the collision point is killed when escaping from the external boundary or Russian roulette game, the calculation for Eq. (5) is terminated. Then, the suspended fixed source calculation is resumed as if nothing had happened. This process is repeated until desired statistics for the flux difference are reached.

Next, how to define the source term in Eq. (5) in the Monte Carlo method is discussed. Once a particle with a weight of W undergoes a collision in the perturbed region in the *unperturbed* system, the calculation mode is switched to the perturbation calculation mode. The source term in Eq. (5) is defined as follows.

(1) Source term caused by the perturbation of the total coefficient

The first term on the right-hand side of Eq. (4) is caused by the perturbation of the total coefficient. This term is represented by

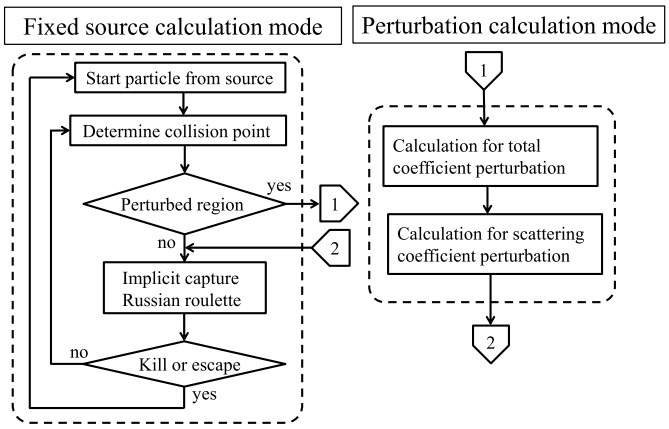

Fig. 1. Schematic flow chart of the perturbation source method.

$$W_t = -\Delta\mu_t(\mathbf{r}, E)\frac{W}{\mu_t(\mathbf{r}, E)}. \tag{6}$$

A new perturbation particle with a weight of W_t is emitted from the collision point. The direction and energy of the new particle are unchanged from the colliding particle. If $\Delta\mu_t > 0$, the weight W_t is negative.

(2) Source term due to the perturbation of the scattering coefficient

The second term on the right-hand side of Eq. (4) is caused by the perturbation of the scattering coefficient. This source term is composed of the perturbation of the total scattering coefficient and the scattering angle and energy distribution function. This source term is obtained by the following steps.

1) The direction $\boldsymbol{\Omega}'$ and energy E' after the scattering are sampled from the probability density function of the *unperturbed* scattering cross section $\mu_s(\mathbf{r}, \boldsymbol{\Omega} \to \boldsymbol{\Omega}', E \to E')$.
2) The source term due to the perturbation of the total scattering coefficient is obtained with

$$W_s = \left(\mu_s^p(\mathbf{r}, E) - \mu_s(\mathbf{r}, E)\right)\frac{W}{\mu_t(\mathbf{r}, E)}, \tag{7}$$

where

$$\mu_s(\mathbf{r}, E) \equiv \int_{4\pi} d\boldsymbol{\Omega}' \int_0^\infty dE' \mu_s\left(\mathbf{r}, \boldsymbol{\Omega} \to \boldsymbol{\Omega}', E \to E'\right), \tag{8}$$

and the superscript p denotes that the quantity is for the perturbed system. Note that the integrals in Eq. (8) are carried out with respect to the angle and energy after scattering.
3) The source term due to the perturbation of the scattering angle and energy distribution is obtained by

$$W_a = \frac{P^p(\boldsymbol{\Omega}', E') - P(\boldsymbol{\Omega}', E')}{P(\boldsymbol{\Omega}', E')}\mu_s^p(\mathbf{r}, E)\frac{W}{\mu_t(\mathbf{r}, E)}, \tag{9}$$

where $P(\boldsymbol{\Omega}', E')$ is the probability density function of the direction $\boldsymbol{\Omega}'$ and the energy E' after scattering in the unperturbed system. Note that Eq. (9) is simply written and it should be modified to use the formatting of the atomic or nuclear data.
4) A new perturbation particle with a weight of $(W_s + W_a)$ is emitted from the collision point. The perturbation particle's direction and energy are $\boldsymbol{\Omega}'$ and E', respectively.

Consequently, the two perturbation particles, which are the sources for the flux difference calculation, are emitted from every collision point, and they are tracked until their deaths. The score of the perturbation particles divided by the total sum of starting particles' weights from the source represents the perturbed flux $\delta\phi(\mathbf{r}, \boldsymbol{\Omega}, E)$. The two perturbation particles are independent and can be emitted in no particular order. A schematic flow chart of this perturbation method is shown in Fig. 1. When the two perturbation particles emitted from the collision point are both killed, the fixed source calculation for Eq. (1) resumes from the collision point. The weights of the perturbation particles for the flux difference calculation are in general smaller than those of the fixed source calculation for Eq. (1) in the unperturbed system, depending on the

perturbation and colliding particle's weight. The lower weight threshold for Eq. (5) should be smaller than the one of the fixed source calculation for Eq. (1) if the Russian roulette game is applied.

As new features of this paper, the performance of the perturbation source method is compared with other Monte Carlo perturbation methods and a method for improving the efficiency is proposed below.

3.2. Improvement of the perturbation source method

As shown in Fig. 1, the perturbation calculation does not start unless the particle undergoes a collision within the perturbed region. Even when the particle enters the perturbed region, the particle that passes through the region without collision does not initiate a perturbation particle. In problems where the perturbed region covers only a small fraction of the whole domain, perturbation particles are rarely emitted, which makes the perturbation calculation less effective. For improving the efficiency of the perturbation source method, a virtual scattering coefficient is added to the perturbed region. The total coefficient μ_t is increased by a factor of $C(>1)$. An increased pseudo total coefficient,

$$\mu_t^* = C \cdot \mu_t, \tag{10}$$

is assigned to the perturbed region. The increased pseudo total coefficient is used for the calculation for the fixed source calculation mode. This method is similar to the Woodcock delta tracking [21] that is used as an efficient algorithm for free path sampling in heterogeneous media. When a particle undergoes a collision within the perturbed region having the pseudo total coefficient μ_t^*, a perturbation particle is emitted from the collision point. The starting weight of the perturbation particle is adjusted to compensate for the biased total coefficient:

$$W_t' = \frac{W_t}{C}, \tag{11}$$

$$W_s' + W_a' = \frac{W_s + W_a}{C}, \tag{12}$$

where W_t, W_s, and W_a are defined by Eqs. (6), (7), and (9), respectively. After the perturbation particles are killed, the perturbation calculation mode is terminated. Then, the fixed source calculation mode is resumed, and a pseudo random number ξ between 0 and 1 is generated. If the random number meets the criteria:

$$\xi < \frac{\mu_t}{\mu_t^*}\left(= \frac{1}{C}\right), \tag{13}$$

the virtual collision in the fixed source calculation mode is accepted as the real collision. If not, the virtual collision is rejected and the random walk continues with the direction, energy, and weight being left unchanged. Whether the virtual collision is accepted or not, the next free path within the perturbed region is sampled with μ_t^*.

4. Numerical tests for the perturbation source method

4.1. Overview of the numerical tests

Numerical tests for the proposed Monte Carlo perturbation method are performed for a two-dimensional 2 cm × 2 cm homogeneous rectangular domain. Following the customary procedure of light transport calculations, the energy dependence is neglected and the scattering angular distribution function is unchanged by the perturbation. The Henyey–Greenstein function [22,23], which is commonly used in light transport calculations, is chosen for the scattering angular distribution function:

$$f(\mathbf{r}, \boldsymbol{\Omega}' \to \boldsymbol{\Omega}) = \frac{1}{4\pi} \frac{1-g^2}{(1+g^2-2g\cos\theta)^{3/2}}, \tag{14}$$

where θ is the angle between $\boldsymbol{\Omega}'$ and $\boldsymbol{\Omega}$, and g is the anisotropy factor. The optical parameters of the unperturbed system are:

$$\mu_s = 10\ \mathrm{cm}^{-1}, \qquad \mu_a = 0.5\ \mathrm{cm}^{-1}, \quad \text{and} \quad g = 0.9,$$

where μ_a = absorption coefficient and $\mu_t = \mu_a + \mu_s = 10.5\ \mathrm{cm}^{-1}$.

As discussed above, the efficiency of the perturbation source method depends on the fraction of the perturbed region. First, the perturbation source method is tested for a perturbation in a larger portion of the whole domain. Then, a perturbation in a smaller portion is tested.

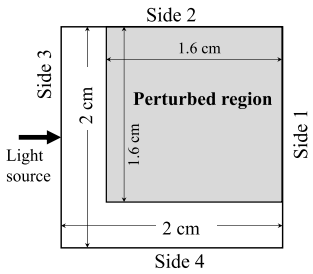

Fig. 2. Geometry for a perturbation in a larger portion.

4.2. Perturbation in a large portion

The absorption coefficient or scattering coefficient is changed in the 1.6 cm $\times$1.6 cm region as shown in Fig. 2. A beam source perpendicular to the "Side 3" is placed at the center of the "Side 3" in Fig. 2. When a particle with a weight of W leaves one of four sides, the boundary measurement of the particle,

$$W \cdot (\mathbf{n} \cdot \boldsymbol{\Omega}), \tag{15}$$

is scored where $\boldsymbol{\Omega}$ = particle's direction and $\mathbf{n}$ = unit outward vector normal to the boundary surface, and the boundary is considered transparent and non-reflecting. The exitance on a side is estimated as

$$P_d = \frac{1}{N}\sum_i W_i \cdot (\mathbf{n} \cdot \boldsymbol{\Omega}_i), \tag{16}$$

where $W_i = i$th particle's weight leaving the side, and i is summed over all particles leaving the side, and $N =$ the total number of particles emitted from the source.

Two perturbations are considered for the numerical tests. In the first one, the absorption coefficient in the perturbed region is increased by 20% (i.e., $+0.1$ cm^{-1}). In the second one, the scattering coefficient is increased by 20% (i.e., $+2.0$ cm^{-1}). To compare the perturbation source method with other perturbation techniques, the correlated sampling method, the first-order differential operator method, and the second-order differential method are used.

In the correlated sampling method used in this paper, the perturbed history is forced to follow the unperturbed one along the same track. When a particle having a weigh of W flies a distance s and undergoes a collision in the perturbed region, the weight of the perturbed history after the collision is [24]

$$W \frac{\mu_t' e^{-\mu_t' s}}{\mu_t e^{-\mu_t s}} \cdot \frac{\mu_s'/\mu_t'}{\mu_s/\mu_t} \cdot \frac{\mu_s}{\mu_t} = W \cdot e^{-\Delta\mu_t s}\frac{\mu_s'}{\mu_t}, \tag{17}$$

where the prime denotes the perturbed coefficient and $\Delta\mu_t = \mu_t' - \mu_t$.

The differential operator method estimates the perturbed exitance with the Taylor series expansion when an optical parameter p changes by Δp:

$$\Delta P_d = \frac{\partial P_d}{\partial p}\Delta p + \frac{1}{2}\frac{\partial^2 P_d}{\partial p^2}\Delta p^2 + \cdots. \tag{18}$$

Cross terms on the second derivative [25] are neglected because the material is single or the perturbation merely changes the density in the examples of this paper.

In the first-order differential operator method, the first-derivative of P_d with respect to μ_a and μ_s in the perturbed region are respectively [26]:

$$\frac{\partial P_d}{\partial \mu_a} = -\frac{1}{N}\sum_i W_i \cdot (\mathbf{n} \cdot \boldsymbol{\Omega}_i) S_i, \tag{19}$$

$$\frac{\partial P_d}{\partial \mu_s} = \frac{1}{N}\sum_i W_i \cdot (\mathbf{n} \cdot \boldsymbol{\Omega}_i)\left(\frac{M_i}{\mu_s} - S_i\right), \tag{20}$$

where $S_i =$ sum of the path lengths in the perturbed region for ith detected particle, and $M_i =$ number of collisions in the perturbed region for ith detected particle. S_i and M_i are accumulated during the course of the random walk in the fixed source Monte Carlo calculation with the unperturbed optical parameters. Similarly, the second-derivative of P_d with respect to μ_a and μ_s in the perturbed region are respectively [26]:

Table 1a
Change of P_d by 20% increase in absorption coefficient in a larger portion.

	Side 1	Side 2	Side 3	Side 4
Independent run	−8.50E−3[a]	−7.09E−3	−3.11E−3	−4.95E−3
	(2.35E−6)[b]	(2.74E−6)	(4.04E−6)	(2.79E−6)
Correlated sampling	−8.50E−3	−7.09E−3	−3.11E−3	−4.95E−3
	(1.11E−6)	(9.47E−7)	(5.21E−7)	(6.86E−7)
Perturbation source $C = 1$	−8.49E−3	−7.09E−3	−3.11E−3	−4.95E−3
	(1.78E−6)	(1.65E−6)	(7.14E−7)	(1.01E−6)
Perturbation source $C = 4$	−8.50E−3	−7.09E−3	−3.11E−3	−4.95E−3
	(2.89E−6)	(2.64E−6)	(9.06E−7)	(1.37E−6)
Differential operator first order	−9.48E−3	−7.85E−3	−3.40E−3	−5.37E−3
	(1.23E−6)	(1.05E−6)	(5.27E−7)	(7.45E−7)
Differential operator second order	−8.41E−3	−7.02E−3	−3.08E−3	−4.92E−3
	(1.10E−6)	(9.40E−7)	(5.17E−7)	(6.82E−7)

[a] Read as -8.50×10^{-3}.
[b] One standard deviation.

Table 1b
Relative FOM with respect to the correlated sampling method for 20% increase in absorption coefficient in a larger portion.

	Side 1	Side 2	Side 3	Side 4
Independent run	0.007	0.004	0.001	0.002
Correlated sampling	1.000	1.000	1.000	1.000
Perturbation source $C = 1$	0.465	0.396	0.641	0.555
Perturbation source $C = 4$	0.132	0.116	0.298	0.226
Differential operator first order	0.812	0.821	0.830	0.848
Differential operator second order	1.08	1.08	1.08	1.07

$$\frac{\partial^2 P_d}{\partial \mu_a^2} = \frac{1}{N}\sum_i W_i \cdot (\mathbf{n}\cdot\boldsymbol{\Omega}_i) S_i^2, \tag{21}$$

$$\frac{\partial^2 P_d}{\partial \mu_s^2} = \frac{1}{N}\sum_i W_i \cdot (\mathbf{n}\cdot\boldsymbol{\Omega}_i)\left(-\frac{M_i}{\mu_s^2} + \left(\frac{M_i}{\mu_s} - S_i\right)^2\right). \tag{22}$$

(1) Perturbation of absorption coefficient

The change of P_d due to the change of the absorption coefficient by +20% are obtained by the four perturbation methods (correlated sampling, perturbation source, first-order, and second-order differential operator methods) and are shown in Table 1a. In addition to the Monte Carlo perturbation methods, the change of P_d is obtained by the difference between two independent runs before and after the perturbation. For the perturbation source method, the factor C defined in Eq. (10) is chosen as $C = 1$ and 4. Throughout this paper, the change of P_d calculated by the perturbation source method agrees with that by the correlated sampling method within 2 standard deviations. The results obtained by the first-order differential operator method significantly differs from other methods. However, the second-order differential operator method performs much better than the first order.

Table 1b compares the relative figure-of-merit (FOM) defined by

$$\mathrm{FOM} = \frac{1}{s^2 T}, \tag{23}$$

where $s =$ one standard deviation of absolute uncertainty and $T =$ computation time. The FOMs are normalized with respect to the correlated sampling. The perturbation source method is less effective compared to other perturbation methods regardless of the factor C. Furthermore, the computation efficiency of the perturbation source method decreases with the factor C, which is contrary to expectation. The additional computational cost for handling more perturbation particles may not be worth the gain of reducing the uncertainty for this problem.

(2) Perturbation of scattering coefficient

The Monte Carlo perturbation calculations due to the perturbation of the scattering coefficient have larger variances than the absorption coefficient. In the first-order differential operator method, for example, this is because two terms, in the parentheses in Eq. (20), M_i/μ_s and S_i, almost cancel each other. The change of P_d due to the change of the scattering coefficient by +20% and the relative FOMs are shown in Tables 2a and 2b, respectively. In this case, the second-order

Table 2a
Change of P_d by 20% increase in scattering coefficient in a larger portion.

	Side 1	Side 2	Side 3	Side 4
Independent run	−8.43E−3[a]	−1.57E−3	5.96E−3	5.58E−4
	(2.39E−6)[b]	(2.86E−6)	(4.14E−6)	(2.89E−6)
Correlated sampling	−8.43E−3	−1.57E−3	5.96E−3	5.51E−4
	(4.88E−6)	(4.88E−6)	(3.68E−6)	(4.11E−6)
Perturbation source $C = 1$	−8.41E−3	−1.52E−3	5.96E−3	5.32E−4
	(3.10E−5)	(2.93E−5)	(2.19E−5)	(2.68E−5)
Perturbation source $C = 4$	−8.45E−3	−1.61E−3	5.98E−3	5.46E−4
	(2.26E−5)	(2.13E−5)	(1.56E−5)	(1.91E−5)
Differential operator first order	−9.73E−3	−1.29E−3	6.08E−3	9.43E−4
	(6.00E−6)	(5.02E−6)	(3.14E−6)	(4.00E−6)
Differential operator second order	−8.24E−3	−1.65E−3	5.96E−3	5.05E−4
	(4.95E−6)	(4.95E−6)	(3.65E−6)	(4.14E−6)

[a] Read as -8.43×10^{-3}.
[b] One standard deviation.

Table 2b
Relative FOM with respect to the correlated sampling method for 20% increase in scattering coefficient in a larger portion.

	Side 1	Side 2	Side 3	Side 4
Independent run	0.138	0.097	0.026	0.067
Correlated sampling	1.000	1.000	1.000	1.000
Perturbation source $C = 1$	0.019	0.021	0.021	0.018
Perturbation source $C = 4$	0.019	0.021	0.022	0.019
Differential operator first order	0.702	0.999	1.46	1.11
Differential operator second order	1.03	1.03	1.08	1.04

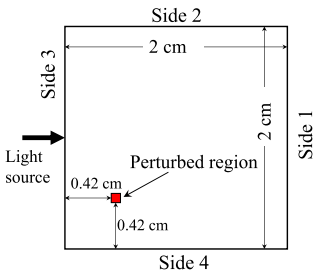

Fig. 3. Geometry for a perturbation in a smaller portion.

differential operator method does not perform as well as with the perturbation of the absorption coefficient. Higher-order derivatives would be required to obtain more accurate estimates using the differential operator method. The FOMs of the perturbation source method for the scattering coefficient are much worse than for the absorption coefficient. The factor C does not affect the efficiency of the perturbation source method unlike the perturbation of the absorption coefficient.

As a conclusion, the source perturbation method can certainly yield an exact estimate of the perturbation. However, for a perturbation in a larger portion of the whole domain, the efficiency is inferior to other Monte Carlo perturbation methods.

4.3. Perturbation in a small portion

The absorption coefficient or scattering coefficient is changed in the 0.0833 cm × 0.0833 cm region as shown in Fig. 3. Again, a beam source perpendicular to the "Side 3" is placed at the center of the "Side 3". The perturbed area within the whole domain accounts for 0.17% of the whole domain. First, a smaller perturbation is added to the perturbed region. According to [4], the correlated sampling method suffers from a large or unbounded variance for a large perturbation. Therefore, a larger perturbation is also tested to compare the efficiency of the perturbation source method to the correlated sampling method.

(1) Smaller perturbation of absorption coefficient

The absorption coefficient in the perturbed region is increased by 20% (i.e., $+0.1\ \mathrm{cm}^{-1}$). The correlated sampling method, the perturbation source method ($C = 1$, 4, and 32), the first-order differential operator method, and the second-order differential method are performed for the perturbation calculation, the change of P_d and their relative FOMs are shown in

Table 3a
Change of P_d by 20% increase in absorption coefficient in a smaller portion.

	Side 1	Side 2	Side 3	Side 4
Correlated sampling	−2.15E−6[a]	−1.47E−6	−1.67E−5	−4.33E−5
	(3.42E−9)[b]	(2.78E−9)	(1.22E−9)	(2.11E−9)
Perturbation source $C = 1$	−2.15E−6	−1.46E−6	−1.67E−5	−4.33E−5
	(3.11E−9)	(2.27E−9)	(1.20E−8)	(2.38E−8)
Perturbation source $C = 4$	−2.15E−6	−1.46E−6	−1.67E−5	−4.33E−5
	(1.62E−9)	(1.18E−9)	(7.54E−9)	(1.59E−8)
Perturbation source $C = 32$	−2.14E−6	−1.46E−6	−1.67E−5	−4.32E−5
	(1.06E−9)	(7.60E−10)	(7.92E−9)	(1.80E−8)
Differential operator first order	−2.16E−6	−1.48E−6	−1.68E−5	−4.35E−5
	(3.45E−9)	(2.81E−9)	(1.24E−8)	(2.18E−8)
Differential operator second order	−2.15E−6	−1.46E−6	−1.68E−5	−4.33E−5
	(3.45E−9)	(2.78E−9)	(1.23E−8)	(2.11E−8)

[a] Read as -2.15×10^{-6}.
[b] One standard deviation.

Table 3b
Relative FOM with respect to the correlated sampling method for 20% increase in absorption coefficient in a smaller portion.

	Side 1	Side 2	Side 3	Side 4
Correlated sampling	1.00	1.00	1.00	1.00
Perturbation source $C = 1$	1.12	1.39	0.960	0.726
Perturbation source $C = 4$	3.83	4.78	2.26	1.50
Perturbation source $C = 32$	11.9	15.3	2.73	1.56
Differential operator first order	0.983	0.982	0.981	0.987
Differential operator second order	0.997	1.01	0.998	1.00

Table 4a
Change of P_d by 300% increase in absorption coefficient in a smaller portion.

	Side 1	Side 2	Side 3	Side 4
Correlated sampling	−2.95E−5[a]	−1.99E−5	−2.30E−4	−6.05E−4
	(4.61E−8)[b]	(3.63E−8)	(1.64E−7)	(2.92E−7)
Perturbation source $C = 1$	−2.96E−4	−1.99E−5	−2.31E−4	−6.05E−4
	(4.35E−8)	(3.12E−8)	(1.67E−7)	(3.36E−7)
Perturbation source $C = 4$	−2.95E−4	−1.98E−5	−2.30E−4	−6.05E−4
	(2.25E−8)	(1.61E−8)	(1.05E−7)	(2.24E−7)
Perturbation source $C = 32$	−2.95E−4	−1.99E−5	−2.31E−4	−6.05E−4
	(1.34E−8)	(9.45E−9)	(1.00E−7)	(2.31E−7)
Differential operator first order	−3.23E−4	−2.21E−5	−2.53E−4	−3.53E−4
	(5.15E−8)	(4.19E−8)	(1.85E−7)	(3.18E−7)
Differential operator second order	−2.92E−4	−1.96E−5	−2.28E−4	−6.02E−4
	(4.53E−8)	(3.56E−8)	(1.62E−7)	(2.90E−7)

[a] Read as -2.95×10^{-5}.
[b] One standard deviation.

Tables 3a, and 3b, respectively. For this perturbation, the estimates of the first-order differential operator method agree with other perturbation methods within 2%, which is much better than the results for the larger perturbation. The efficiency of the perturbation source method with $C = 1$ is improved in the two sides and worsened in the remaining two sides compared with other perturbation methods. The efficiency of the perturbation source method becomes better as C increases. By adjusting the factor C, the perturbation source method can be superior to other Monte Carlo perturbation techniques.

(2) Larger perturbation of absorption coefficient

The absorption coefficient in the perturbed region is increased by 300% (i.e., $+1.5$ cm^{-1}). The results are shown in Tables 4a, and 4b. The tendency of the relative FOMs in Table 4b is almost the same as the smaller perturbation in Table 3b.

(3) Smaller perturbation of scattering coefficient

The scattering coefficient in the perturbed region is increased by 30% (i.e., $+3.0$ cm^{-1}). The results are shown in Tables 5a, and 5b. The perturbed source method with $C = 1$ is approximately half as effective as the correlated sampling

Table 4b
Relative FOM with respect to the correlated sampling method for 300% increase in absorption coefficient in a smaller portion.

	Side 1	Side 2	Side 3	Side 4
Correlated sampling	1.00	1.00	1.00	1.00
Perturbation source $C = 1$	1.08	1.30	0.930	0.725
Perturbation source $C = 4$	3.73	4.51	2.21	1.51
Perturbation source $C = 32$	11.9	14.7	2.70	1.59
Differential operator first order	0.832	0.782	0.821	0.876
Differential operator second order	1.03	1.04	1.03	1.01

Table 5a
Change of P_d by 30% increase in scattering coefficient in a smaller portion.

	Side 1	Side 2	Side 3	Side 4
Correlated sampling	5.46E−6[a]	4.95E−6	2.51E−5	−6.89E−5
	(9.99E−8)[b]	(7.65E−8)	(3.52E−7)	(6.10E−7)
Perturbation source $C = 1$	5.71E−6	5.07E−6	2.47E−5	−6.90E−5
	(1.37E−7)	(9.98E−8)	(4.37E−7)	(7.19E−7)
Perturbation source $C = 4$	5.60E−6	5.05E−6	2.51E−5	−6.89E−5
	(6.70E−8)	(5.00E−8)	(2.16E−7)	(3.63E−7)
Perturbation source $C = 32$	5.60E−6	4.99E−6	2.50E−5	−6.89E−5
	(3.06E−8)	(2.29E−8)	(1.03E−7)	(1.79E−7)
Differential operator first order	5.91E−6	5.07E−6	2.50E−5	−7.01E−5
	(9.98E−8)	(7.45E−8)	(3.52E−7)	(6.34E−7)
Differential operator second order	5.71E−6	5.01E−6	2.46E−5	−6.87E−5
	(1.01E−7)	(7.69E−8)	(3.51E−7)	(6.11E−7)

[a] Read as 5.46×10^{-6}.
[b] One standard deviation.

Table 5b
Relative FOM with respect to the correlated sampling method for 30% increase in scattering coefficient in a smaller portion.

	Side 1	Side 2	Side 3	Side 4
Correlated sampling	1.00	1.00	1.00	1.00
Perturbation source $C = 1$	0.515	0.544	0.621	0.666
Perturbation source $C = 4$	1.85	1.95	2.22	2.36
Perturbation source $C = 32$	7.19	7.56	7.97	7.84
Differential operator first order	1.14	1.20	1.14	1.05
Differential operator second order	1.02	1.03	1.05	1.04

method. However, the efficiency of the perturbed source method increases with the factor C. When $C = 32$, the perturbation source method outperforms the correlated sampling method by a factor of 7. The perturbation source method can achieve a higher efficiency than other perturbation methods by adjusting the factor C.

(4) Larger perturbation of scattering coefficient

The scattering coefficient in the perturbed region is increased by 200% (i.e., $+20.0$ cm^{-1}). The results are shown in Tables 6a, and 6b. For such a larger perturbation of the scattering coefficient, the correlated sampling method incurs a larger variance, which can be observed by comparing the FOMs between the correlated sampling method and the differential operator method. Thus, the perturbation source method and the differential operator method exhibit relatively better performance than the correlated sampling method. The improvement of the efficiency in the perturbation source method is more remarkable than in the smaller perturbation. When $C = 32$, the perturbation source method is about 50 times more efficient than the correlated sampling method.

4.4. Perturbation in an anisotropy factor

In the next example, the anisotropy factor of the Henyey–Greenstein function, which is defined in Eq. (14), is perturbed in the perturbed region in Fig. 3. The correlated sampling method, the perturbation source method ($C = 1$, 4, and 32), the first-order differential operator method, and the second-order differential method are tested for the perturbation calculation.

In the perturbation source method, when a particle having a weight of W undergoes a collision within the perturbed region, a perturbation particle is emitted from the collision point. The scattering angle θ for the perturbation particle is sampled using Eq. (14). The weight of the perturbation particle emitted from the collision point is:

Table 6a
Change of P_d by 200% increase in scattering coefficient in a smaller portion.

	Side 1	Side 2	Side 3	Side 4
Correlated sampling	3.26E−5[a]	2.89E−5	1.39E−4	−4.15E−4
	(1.69E−6)[b]	(1.26E−6)	(7.67E−6)	(1.27E−5)
Perturbation source $C = 1$	3.38E−5	3.17E−5	1.55E−4	−4.21E−4
	(9.36E−7)	(7.11E−7)	(3.29E−6)	(5.71E−6)
Perturbation source $C = 4$	3.31E−5	3.17E−5	1.53E−4	−4.17E−4
	(4.68E−7)	(3.56E−7)	(1.65E−6)	(2.86E−6)
Perturbation source $C = 32$	3.31E−5	3.22E−5	1.54E−4	−4.20E−4
	(1.65E−7)	(1.26E−7)	(5.82E−7)	(1.01E−6)
Differential operator first order	3.77E−5	3.45E−5	1.71E−4	−4.64E−4
	(6.46E−7)	(4.83E−7)	(2.27E−6)	(4.10E−6)
Differential operator second order	3.26E−5	3.18E−5	1.58E−4	−4.14E−4
	(1.20E−6)	(1.00E−6)	(4.22E−6)	(6.40E−6)

[a] Read as 3.26×10^{-5}.
[b] One standard deviation.

Table 6b
Relative FOM with respect to the correlated sampling method for 200% increase in scattering coefficient in a smaller portion.

	Side 1	Side 2	Side 3	Side 4
Correlated sampling	1.00	1.00	1.00	1.00
Perturbation source $C = 1$	3.01	2.93	5.03	4.54
Perturbation source $C = 4$	10.8	10.5	18.1	16.4
Perturbation source $C = 32$	41.3	40.1	69.1	62.3
Differential operator first order	7.11	7.14	11.9	9.94
Differential operator second order	2.04	1.66	3.45	4.07

$$W_a = \frac{f(\theta, g') - f(\theta, g)}{f(\theta, g)} \mu_s^p \frac{W}{\mu_t}, \tag{24}$$

where $g' =$ the perturbed anisotropy factor, and

$$f(\theta, g) = \frac{1}{4\pi} \frac{1 - g^2}{(1 + g^2 - 2g\cos\theta)^{3/2}}. \tag{25}$$

In the correlated sampling method, when a particle having a weight of W flies a distance s and undergoes a collision in the perturbed region, the weight of the perturbed history after the collision is

$$W \cdot e^{-\Delta\mu_t s} \frac{\mu_s}{\mu_t} \cdot \frac{f(\theta, g')}{f(\theta, g)}, \tag{26}$$

where $\theta =$ the scattering angle for the perturbed and unperturbed histories after the collision.

In the differential operator method, the first- and the second-derivative of P_d with respect to the anisotropy factor g in the perturbed region are respectively [26]:

$$\frac{\partial P_d}{\partial g} = \frac{1}{N} \sum_i W_i \cdot (\mathbf{n} \cdot \boldsymbol{\Omega}_i) G_{1i}, \tag{27}$$

$$\frac{\partial^2 P_d}{\partial g^2} = \frac{1}{N} \sum_i W_i \cdot (\mathbf{n} \cdot \boldsymbol{\Omega}_i) \left(G_{1i}^2 + G_{2i}\right), \tag{28}$$

where

$$G_{1i} = \sum_j \frac{1}{f(\theta_j, g)} \frac{\partial f(\theta_j, g)}{\partial g}, \tag{29}$$

$$G_{2i} = \sum_j \frac{\partial}{\partial g} \left(\frac{1}{f(\theta_j, g)} \frac{\partial f(\theta_j, g)}{\partial g} \right), \tag{30}$$

and the summation symbols for j denote the sum for all collisions in the perturbed region.

The perturbation calculations are performed when the anisotropy factor g is changed from 0.9 to 0.895. The change of P_d and their relative FOMs are shown in Tables 7a, and 7b, respectively. The perturbed source method with $C = 1$ is as effective as other perturbation methods for this perturbation. However, the efficiency of the perturbation source method

Table 7a
Change of P_d by the change of the anisotropy factor from 0.9 to 0.895.

	Side 1	Side 2	Side 3	Side 4
Correlated sampling	9.05E−7[a]	8.71E−7	4.19E−6	−1.15E−5
	(1.49E−8)[b]	(1.14E−8)	(5.25E−8)	(9.18E−8)
Perturbation source $C = 1$	9.16E−7	8.70E−7	4.16E−6	−1.14E−5
	(1.49E−8)	(1.13E−8)	(5.26E−8)	(9.17E−8)
Perturbation source $C = 4$	9.04E−7	8.54E−7	4.14E−6	−1.15E−5
	(7.48E−9)	(5.69E−9)	(2.65E−8)	(4.64E−8)
Perturbation source $C = 32$	9.16E−7	8.58E−7	4.17E−6	−1.14E−5
	(2.66E−9)	(2.02E−9)	(9.95E−9)	(1.82E−8)
Differential operator first order	9.29E−7	8.63E−7	4.18E−6	−1.14E−5
	(1.08E−8)	(8.18E−9)	(3.80E−8)	(6.71E−8)
Differential operator second order	8.92E−7	8.70E−7	4.09E−6	−1.15E−5
	(9.62E−9)	(7.36E−9)	(3.39E−8)	(5.92E−8)

[a] Read as 9.05×10^{-7}.
[b] One standard deviation.

Table 7b
Relative FOM with respect to the correlated sampling method for the change of the anisotropy factor from 0.9 to 0.895.

	Side 1	Side 2	Side 3	Side 4
Correlated sampling	1.00	1.00	1.00	1.00
Perturbation source $C = 1$	1.00	1.02	0.997	1.00
Perturbation source $C = 4$	3.69	3.74	3.65	3.63
Perturbation source $C = 32$	18.6	18.9	16.5	15.0
Differential operator first order	1.00	1.01	0.994	0.974
Differential operator second order	1.04	1.04	1.04	1.04

Table 8a
Change of P_d by the change of the anisotropy factor from 0.9 to 0.6.

	Side 1	Side 2	Side 3	Side 4
Correlated sampling	4.27E−5[a]	4.87E−5	2.05E−4	−5.68E−4
	(7.94E−7)[b]	(8.57E−7)	(3.74E−6)	(3.62E−6)
Perturbation source $C = 1$	4.17E−5	4.95E−5	2.06E−4	−5.70E−4
	(4.35E−7)	(3.90E−7)	(1.54E−6)	(1.92E−6)
Perturbation source $C = 4$	4.24E−5	4.91E−5	2.05E−4	−5.68E−4
	(2.69E−7)	(2.39E−7)	(9.51E−7)	(1.21E−6)
Perturbation source $C = 32$	4.25E−5	4.97E−5	2.06E−4	−5.69E−4
	(1.07E−7)	(9.51E−8)	(4.05E−7)	(5.83E−7)
Differential operator first order	5.23E−5	5.14E−5	2.49E−4	−6.92E−4
	(9.11E−7)	(6.93E−7)	(3.23E−6)	(5.69E−6)
Differential operator second order	4.15E−5	5.00E−5	1.89E−4	−5.75E−4
	(2.67E−6)	(2.11E−6)	(9.52E−6)	(1.69E−5)

[a] Read as 4.27×10^{-5}.
[b] One standard deviation.

Table 8b
Relative FOM with respect to the correlated sampling method for the change of the anisotropy factor from 0.9 to 0.6.

	Side 1	Side 2	Side 3	Side 4
Correlated sampling	1.00	1.00	1.00	1.00
Perturbation source $C = 1$	3.70	5.46	6.66	4.00
Perturbation source $C = 4$	13.2	19.5	23.5	13.6
Perturbation source $C = 32$	69.0	102	107	48.4
Differential operator first order	1.39	2.80	2.45	0.742
Differential operator second order	0.162	0.301	0.283	0.0841

increases with the factor C. Tables 8a and 8b show the results when the perturbation of g is much larger (from 0.9 to 0.6). For the perturbation of g, the perturbation source method outperforms other perturbation methods regardless of the factor C.

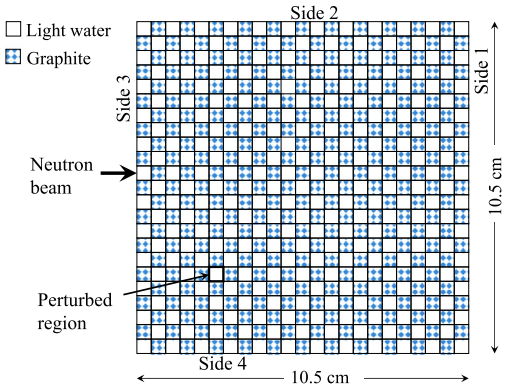

Fig. 4. Geometry for a multi-group neutron transport perturbation.

Table 9
3-group constants for light-water and graphite.

		Light-water	Graphite
Σ_{t1} (cm^{-1})	Total cross section of 1st group	0.33207	0.21053
Σ_{t2} (cm^{-1})	Total cross section of 2nd group	1.1265	0.45009
Σ_{t3} (cm^{-1})	Total cross section of 3rd group	2.7812	0.53500
Σ_{a1} (cm^{-1})	Absorption cross section of 1st group	0.00030500	0.00013890
Σ_{a2} (cm^{-1})	Absorption cross section of 2nd group	0.00036990	0.0000017
Σ_{a3} (cm^{-1})	Absorption cross section of 3rd group	0.018250	0.000021
$\Sigma_s^{1\to2}$ (cm^{-1})	Group-transfer cross section from 1st to 2nd group	0.10464	0.029672
$\Sigma_s^{2\to3}$ (cm^{-1})	Group-transfer cross section from 2nd to 3rd group	0.097961	0.015913

Table 10a
Change of the thermal neutron currents by 80% decrease in the light water density.

	Side 1	Side 2	Side 3	Side 4
Correlated sampling	−6.56E−5[a]	−7.71E−5	−1.74E−4	2.01E−5
	(1.78E−6)[b]	(1.17E−6)	(3.82E−6)	(5.84E−6)
Perturbation source $C = 1$	−6.45E−5	−7.68E−5	−1.67E−4	6.02E−6
	(4.02E−7)	(8.63E−7)	(2.14E−6)	(2.15E−6)
Perturbation source $C = 10$	−6.46E−5	−7.65E−5	−1.70E−4	8.99E−6
	(8.65E−7)	(4.01E−7)	(1.02E−6)	(1.03E−6)
Perturbation source $C = 30$	−6.48E−5	−7.66E−5	−1.68E−4	7.73E−6
	(3.68E−7)	(3.67E−7)	(9.87E−7)	(9.92E−7)
Differential operator first order	−5.22E−5	−6.25E−5	−1.57E−4	−1.61E−5
	(6.90E−7)	(6.90E−7)	(2.05E−6)	(2.06E−6)
Differential operator second order	−6.23E−5	−7.49E−5	−1.62E−4	−5.09E−6
	(8.89E−7)	(8.87E−7)	(2.74E−6)	(2.74E−6)

[a] Read as -6.56×10^{-5}.
[b] One standard deviation.

4.5. Perturbation for multi-group neutron transport in a heterogeneous geometry

The perturbation source method is applied to perturbation calculations for multi-group neutron transport in a heterogeneous geometry. The geometry for the perturbation calculations is a two-dimensional right square having a checkerboard pattern array of light water and graphite as shown in Fig. 4. The calculations use 3 energy group constants that are prepared with the standard reactor analysis code SRAC [27]. The constants are listed in Table 9. The scattering is assumed to be isotropic. A line neutron beam in the 1st energy group perpendicular to the "Side 3" enters from the center of the "Side 3". As the perturbation added to this configuration, the water density of the perturbed region decreases by 80%. In the same manner as in the numerical examples shown above, the changes of the neutron currents in the 3rd energy group (i.e., thermal neutron) on the four outer boundaries are calculated with the three perturbation methods. The change of the thermal neutron currents and their relative FOMs are shown in Tables 10a, and 10b, respectively. Among the perturbation methods tested in this paper, the computation efficiency is maximized when the perturbation source method with $C \approx 30$ is used. The tendency for this neutron transport in the heterogeneous geometry is the same as the numerical examples for the light transport.

Table 10b
Relative FOM with respect to the correlated sampling method for 80% decrease in the light water density.

	Side 1	Side 2	Side 3	Side 4
Correlated sampling	1.00	1.00	1.00	1.00
Perturbation source $C = 1$	6.18	2.71	4.64	10.8
Perturbation source $C = 10$	19.7	8.62	14.0	32.6
Perturbation source $C = 30$	23.6	10.3	15.0	34.9
Differential operator first order	12.5	5.45	6.50	15.2
Differential operator second order	7.08	3.09	3.43	8.01

5. Conclusions

The present paper has proposed an exact Monte Carlo perturbation method for fixed source problems, which is dubbed the "perturbation source method". This paper is actually an improvement over a previously proposed version of the perturbation source method. In the previous studies for the perturbation source method, the higher-order perturbation has been neglected and the accuracy has been limited within the first-order perturbation. On the other hand, the perturbation source method in this paper solves explicitly and exactly the transport equation for the flux difference without approximation by tracking "perturbation particles" in the perturbed system. This method employs a quite different concept from the well-known perturbation methods such as the correlated sampling method and the differential operator method. This method requires the flux in the unperturbed system as its source term. The unperturbed flux is provided by an "on-the-fly" technique during the course of the ordinary fixed source calculation for the unperturbed system. Then, a perturbation particle that started from the collision point in the perturbed region is tracked until its death.

If the perturbed region covers a larger portion of the whole domain, too many perturbation particles have to be tracked, which makes the perturbation source method less effective than the correlated sampling method. On the other hand, if the perturbed region covers only a smaller portion of the whole domain, too few perturbation particles are started. For a perturbation in a smaller portion, the efficiency of the perturbation source method can be improved by adding a virtual scattering coefficient to the perturbed region, forcing collisions in the perturbed region.

The numerical tests are performed for a particle transport in a two-dimensional semi-transparent material. The numerical tests in this paper compare the perturbation source method with the correlated sampling method, the first-order differential operator method, and the second-order differential operator method. The perturbation source method is less effective than the correlated sampling method for a perturbation in a larger portion of the whole domain. However, the perturbation source method outperforms other perturbation methods in situations where the perturbed region covers only a smaller portion of the whole domain. The improvement by the perturbation source method depends on the added virtual scattering coefficient or cross section and on how large the perturbation is. For a large perturbation, the correlated sampling method suffers from a large variance. In such a case, the performance of the perturbation source method is relatively superior to the correlated sampling method. The efficiency of the perturbation source method depends strongly on the adjustment of the virtual scattering coefficient or cross section added to the perturbed region. As a general rule, the efficiency increases with the virtual scattering coefficient added.

There still remain some works to be done in the future. The application to the continuous-energy physics is one of future works. The optimization of the factor C for increasing the number of collisions in a perturbed region may also be desirable. The proposed method can be straightforwardly applied to k_{eff}-eigenvalue problems unless the fission source distribution is changed by a perturbation. However, a new algorithm should be invented to take into account the fission source perturbation.

References

[1] J. Spanier, E.M. Gelbard, Monte Carlo Principles and Neutron Transport Problems, Addison-Wesley Publishing Company, 1969.
[2] W. Bernnat, A Monte Carlo Technique for Local Perturbations in Multiplying Systems, Argonne National Laboratory, 1974, ANL-75-2.
[3] M. Nakagawa, T. Asaoka, Improvement of correlated sampling Monte Carlo methods for reactivity calculations, J. Nucl. Sci. Technol. 15 (1978) 400.
[4] H. Rief, Generalized Monte Carlo perturbation algorithms for correlated sampling and a second-order Taylor series approach, Ann. Nucl. Energy 9 (1984) 455–476.
[5] T. Kitada, A. Yamane, T. Takeda, Improvements of correlated sampling method in Monte Carlo perturbation theory, in: Proc. Int. Conf. on the Physics of Reactors PHYSOR96, Mito, Ibaraki, Japan, Sep. 16–20, 1996, 1996, pp. A-212–A-219.
[6] J.E. Olhoeft, The Doppler Effect for a Non-Uniform Temperature Distribution in Reactor Fuel Elements, Westinghouse Electric Corporation, 1962, WCAP-2048.
[7] H. Takahashi, Monte Carlo method for geometrical perturbation and its application to the pulsed fast reactor, Nucl. Sci. Eng. 41 (1970) 259–279.
[8] Y. Nagaya, T. Mori, Impact of perturbed fission source on the effective multiplication factor in Monte Carlo perturbation calculations, J. Nucl. Sci. Technol. 42 (2005) 428–441.
[9] Y. Nagaya, T. Mori, Estimation of sample reactivity worth with differential operator sampling method, Prog. Nucl. Sci. Technol. 2 (2011) 842–850.
[10] T. He, B. Su, On using correlated sampling to simulate small changes in system response by MCNP, Ann. Nucl. Energy 37 (2010) 34–42.
[11] T. He, B. Su, Comparison between correlated sampling and the perturbation technique of MCNP5 for fixed-source problems, Ann. Nucl. Energy 38 (2011) 1318–1326.
[12] J.D. Densmore, G.W. McKinney, J.S. Hendricks, Correction to the MCNP Perturbation Feature for Cross-Section Dependent Tallies, 1997, LA-13374.

[13] G.W. McKinney, J.L. Iverson, Verification of the Monte Carlo Differential Operator Technique for MCNP, Los Alamos National Laboratory, 1996, LA-13098.
[14] J.A. Favorite, An alternative implementation of the differential operator (Taylor series) perturbation methods for Monte Carlo criticality problems, Nucl. Sci. Eng. 142 (2002) 327–341.
[15] H.J. Shim, C.H. Kim, Adjoint sensitivity and uncertainty analyses in Monte Carlo forward calculations, J. Nucl. Sci. Technol. 48 (2011) 1453–1461.
[16] H.J. Shim, B.S. Han, J.S. Jung, H.J. Park, C.H. Kim, McCARD: Monte Carlo code for advance reactor design and analysis, Nucl. Eng. Technol. 44 (2012) 161–176.
[17] K.F. Raskach, An improvement of the Monte Carlo generalized differential operator method by taking into account first- and second-order perturbations of fission source, Nucl. Sci. Eng. 162 (2009) 158–166.
[18] I. Lux, L. Koblinger, Monte Carlo Particle Transport Methods: Neutron and Photon Calculations, CRC Press, 1991.
[19] W. Matthes, Calculation of reactivity perturbations with the Monte Carlo method, Nucl. Sci. Eng. 47 (1972) 234–237.
[20] W.E. Preeg, J.S.K. Tsang, Comparison of correlated Monte Carlo techniques, Trans. Am. Nucl. Soc. 43 (1982) 628–629.
[21] E.R. Woodcock, Techniques used in the GEM Code for Monte Carlo Neutronics Calculations in Reactors and Other Systems of Complex Geometry, Argonne National Laboratory, 1965, ANL-7050.
[22] S.A. Prahl, M. Kaijzer, S.L. Jacques, A.J. Welch, A Monte Carlo model of light propagation in tissue, SPIE Inst. Ser. IS 5 (1989) 102–111.
[23] L.C. Henyey, J.L. Greenstein, Diffuse radiation in the galaxy, Astrophys. J. 93 (1941) 70–83.
[24] C. Zhu, Q. Liu, Review of Monte Carlo modeling of light transport in tissue, J. Biomed. Opt. 18 (5) (2013) 050902.
[25] J.A. Favorite, D.K. Parsons, Second-order cross terms in Monte Carlo differential operator perturbation estimates, in: Proc. M&C 2001, Salt Lake City, Utah, 2001.
[26] Y. Nagaya, Ph.D. Dissertation, Kyoto University, 2012 (in Japanese).
[27] K. Okumura, T. Kugo, K. Kaneno, K. Tsuchihashi, SRAC2006: a comprehensive neutronics calculation code system, in: JAEA-Data/Code 2007-004, 2007.